HAL
archives-ouvertes.fr

Toward High-Dimensional Single-Cell Analysis of Graphene Oxide Biological Impact: Tracking on Immune Cells by Single-Cell Mass Cytometry

Marco Orecchioni, Valentina Bordoni, Claudia Fuoco, Giacomo Reina, Hazel Lin, Martina Zoccheddu, Acelya Yilmazer, Barbara Zavan, Gianni Cesareni, Davide Bedognetti, et al.

▶ **To cite this version:**

Marco Orecchioni, Valentina Bordoni, Claudia Fuoco, Giacomo Reina, Hazel Lin, et al.. Toward High-Dimensional Single-Cell Analysis of Graphene Oxide Biological Impact: Tracking on Immune Cells by Single-Cell Mass Cytometry. Small, Wiley-VCH Verlag, 2020, 16 (21), pp.2000123. 10.1002/smll.202000123 . hal-03001318

HAL Id: hal-03001318
https://hal.archives-ouvertes.fr/hal-03001318

Submitted on 16 Nov 2020

HAL is a multi-disciplinary open access archive for the deposit and dissemination of scientific research documents, whether they are published or not. The documents may come from teaching and research institutions in France or abroad, or from public or private research centers.

L'archive ouverte pluridisciplinaire **HAL**, est destinée au dépôt et à la diffusion de documents scientifiques de niveau recherche, publiés ou non, émanant des établissements d'enseignement et de recherche français ou étrangers, des laboratoires publics ou privés.

Towards high dimensional single cell analysis of graphene oxide biological impact: tracking on immune cells by single cell mass cytometry

Marco Orecchioni,[1#] Valentina Bordoni,[1#] Claudia Fuoco,[2#] Giacomo Reina,[3] Hazel Lin,[3] Martina Zoccheddu[1], Acelya Yilmazer,[4] Barbara Zavan[5], Gianni Cesareni,[2] Davide Bedognetti,[6] Alberto Bianco,[3] and Lucia Gemma Delogu[1,5,7]*

[1]Department of Chemistry and Pharmacy University of Sassari, Sassari, Italy

[2] Department of Biology, University of Rome Tor Vergata, Rome, Italy

[3] CNRS, Immunology, Immunopathology and Therapeutic Chemistry, UPR 3572, University of Strasbourg, ISIS, 67000 Strasbourg, France

[4]Ankara University Faculty of Engineering, Department of Biomedical Engineering, Ankara, Turkey

[5] University of Padua, Department of Biomedical Sciences, Padova, Italy

[6]Immunology and Therapy Section, Division of Translational Medicine, Sidra Medical and Research Center, Doha, Qatar.

[7]Istituto di Ricerca Pediatrica Città della Speranza, Padova, Italy

*Corresponding authors: a.bianco@ibmc-cnrs.unistra.fr; lgdelogu@uniss.it, luciagemma.delogu@unipd.it

# Equal contributions

Keywords: 2D materials, CyTOF, biocompatibility, Immune cells, safety

Abstract

Considering the potential exposure to graphene, the most investigated nanomaterials, the assessment of the impact on human health has become an urgent need. The deep understanding of nanomaterial safety, is today possible by high-throughput single-cell technologies. Single-cell mass cytometry (CyTOF) shows an unparalleled ability to phenotypically and functionally profile complex cellular systems, in particular related to the immune system, as recently proved also for graphene impact. The next challenge was to track the graphene distribution at the single-cell level. Therefore, graphene oxide (GO) was functionalized with $AgInS_2$ nanocrystals (GO-In), allowing us to trace GO immune-cell interactions via the indium (^{115}In) channel. Indium was chosen specifically to avoid overlaps with the commercial panels (>30 immune markers). As a proof of concept, the GO-In CyTOF tracking was performed at single-cell level on blood immune subpopulations, showing the GO interaction with monocytes and B cells, therefore guiding future immune studies. The proposed approach can be applied not only to the immune safety assessment of the multitude of graphene physical and chemical parameters, but also for graphene applications in neuroscience. Moreover, our approach can be translated to other 2D emerging materials, and will likely advance our understanding of their toxicology.

Graphene, a single layer of hexagonally arranged carbon atoms, is considered the most versatile material available to mankind: the thinnest, the strongest, the lightest, extremely flexible, highly electrically and thermally conductive material [1, 2], a versatile entity for multiple functionalization. Due to its unique combination of superior properties, graphene is the starting platform for new disruptive technologies across a wide range of fields [3, 4] Various graphene-based technologies have now transformed into commercial products, in sports goods, automotive coatings, conductive inks, touch screens and several others [5]. The massive production and use of graphene materials will increase exponentially over the coming years. On the other hand, an ever-growing literature is related to the explorations of graphene materials for new diagnostic and therapeutic strategies [6-9]. The graphene material exposure, due to the different applications, might open possible threats to human health [10], becoming an urgent domain of research to fill in nanotoxicology. In this context, graphene deserves, for its safe exploitation, to stay on the trail of the new technologies that are giving a deeper and deeper understanding of biology [11-15] and complex cell networks. Nanosafety research should provide new insights into a comprehensive picture of graphene material biological interaction considering the cellular, subcellular and single-cell level.

Single-cell technologies are becoming fundamental to decipher the biological impact of nanomaterials with high parameterization [13, 16, 17]. Among other single-cell procedures such as single-cell genomics, transcriptomics and proteomics, we focus here on single-cell mass cytometry, a technique that can clarify cellular identity, function and biological mechanisms in response to different stimuli [13, 14, 18, 19]. Single-cell mass cytometry employs metal element-tagged probes that enable the discrimination of particles according to their mass/charge ratio (*m/z*), with minimal overlap and signal background, enabling high-dimensional analysis of over 100 parameters at the single-cell level with high accuracy [20]. The current

instrumentation for mass cytometry, used in the present, work is called Cytometry by Time-of Flight (CyTOF) [21, 22]. This technique allowed to answer unsolved biological problems and open new scenarios of studies on the entire hematopoietic tree of cell differentiation [23], on the human immune system development and variation [24-26], on the immune cell variation in healthy and tumor tissues [27-29], on the identification of rare antigen-specific cells [30] and on the brain cell populations [31, 32], just to mention some of the breakthrough discoveries thanks to single-cell mass cytometry. As that approach already did in other fields, we believe it will likely revolutionize the field of nanotoxicology,

The study of nanomaterials and specifically graphene material interaction with the immune system is a prerequisite for understanding its safety. The extensive functional heterogeneity of the immune cells and the fact that immunological processes differ substantially among cell subpopulations detectable by a multitude of markers, make them the first ideal cell populations to be studied in single-cell mass cytometry [33].

We previously proposed the use of single-cell mass cytometry to dissect the immunological effects of graphene on human peripheral blood mononuclear cells [17]. Our results emphasized the importance of the functionalization on enhancing the biocompatibility of GO-based materials.

Even though our results helped to shed light on the GO interaction with several immune subpopulations, we were technically unable to trace the graphene-cell interaction linking it to cell population changes in functionality. In fact, carbon-based nanomaterials cannot be detected by mass cytometry [22]. Instead, the group of Irvine and Stellacci successfully proposed the use of single-cell mass spectrometry for the detection of gold nanoparticles [34]. A similar approach was used by Ivask *et al.* and Oliver *et al.* who applied mass cytometry for the detection of silver nanoparticles in T cells and macrophages, respectively [35-37].

In our work, to make graphene material trackable by single-cell mass cytometry, we developed a GO complexed with $AgInS_2$ nanocrystals with a size of 5 nm (called GO-In).

.

The oxidized form of graphene (namely GO) has intrinsic physicochemical properties that make it an unique material [38]. Some of the chemical properties include large surface area, diverse functionalities, and good biocompatibility [8, 39, 40]. These properties of GO allow it to be studied for several applications in nanomedicine, including bioimaging, biosensing and tissue regeneration [41, 42]. However, the increasing use and large-scale production of this material also necessitates careful investigations of its impact on human tissues [39]. The combination of GO with $AgInS_2$ quantum dots was chosen because of the physicochemical properties of the latter, making the complex visible by single cell mass cytometry, and high biocompatibility, proven in several biomedical applications [43, 44].

The functionalization gives GO the unique property to be detected in the indium channel (^{115}In) of the mass spectrometer, allowing the cellular tracking of GO by the high throughput approach of single-cell mass cytometry. The indium was specifically chosen for its compatibility with the major commercial antibody (metal-tagged) panels designed for immune-phenotyping and immune functionality. As a proof of concept, we applied the GO-In property to deconvolute the diversity of immune cell interaction by performing the tracking by CyTOF on the complex pool of human peripheral blood mononuclear cells (PBMCs) from healthy donors (**Figure 1a)**. The high dimensional single-cell graphene tracking analysis can open a new path for immunological safe assessment of a wide variety of nanomaterials in their multiple uses including in the future clinical practice.

GO was prepared by the Hummers' method. We have selected for this work a GO with the lateral size of 300 ± 200 nm [45, 46]. To allow tracking the flakes, GO was covalently labeled with cysteine-capped $AgInS_2$ quantum dots via epoxide opening reaction (**Figure 1b**) [47]. The TEM images of GO-In show the presence of small dark particles (2-5 nm) [47, 48] on GO associated to the $AgInS_2$ (**Figure 1c**), as confirmed by the appearance of In 3d bands in the XPS survey and high resolution spectra (**Figure S1 and S2**). The percentage of In calculated from the XPS survey was 0.29 at% (**Table S1**). We tested the stability of the GO-In adducts in cell

culture media incubated at 37 °C for one week (**Figure S3**) showing no leakage of $AgInS_2$ nanoparticles from the GO flakes. This permit to track ^{115}In from the $AgInS_2$ to follow the fate of GO after interactions with the immune cells.

To track graphene in the different immune cell populations, at single-cell level, PBMCs were treated with GO-In (50 µg/mL) for 24 h, then harvested and stained with the Maxpar Human Peripheral Blood Phenotyping Panel Kit able to give the full picture on 18 distinct immune cell types. Dose and time points were chosen based on previous works on the same types of cells [17].

The immune cell populations were identified according to the expression profile of several clusters of differentiation (CD) markers present on their cell surface.

We analyzed simultaneously 17 markers discriminating the selected 18 subpopulations. GO-In-cell interaction was detected by the indium channel. The ^{115}In channel and the specific GO $AgInS_2$ nanocrystal functionalization, was chosen to avoid overlaps with the Fluidigm Maxpar immune characterization commercial panels containing more than 30 markers.

To construct the single-cell resolution plot, we applied the viSNE computational approach. As a first step, we used nine markers (CD3, CD4, CD8, CD20, CD19, CD14, CD123, CD11c, and CD16) in GO-In treated and untreated healthy human PBMCs. We identified the major immune cell populations among CD45+ cells (**Figure 1d**). Cisplatin (Cis) staining was performed to assess the viability at single-cell level. Cisplatin is a molecule able to enter into the late apoptotic and necrotic cells that have lost membrane integrity. The viSNE analysis showed no Cis signal variation in the GO-In treated cells (**Figure 1d**). The Cis mean intensity analysis among the 3 biological replicates confirmed that no significant variations in terms of viability were present in the treated and untreated samples among the immune cell subpopulations (**Figure 1e**).

Then we examined whether the immune cell subpopulations interact with GO-In. The viSNE plot (**Figure 1f**), the heatmap (**Figure 1g**) and the bar graphs reporting the biological replicates

(**Figure 1h**) show that classical monocytes (C mono) are the main population able to strongly interact with GO-In. Unexpectedly, also B cells interact with GO-In. No other immune cell populations analyzed, including T-helper cells (Th. cells), cytotoxic T cells (Ct. cells), intermediate monocytes (Int. mono), non-classical monocytes (NC mono), natural killer cells (NK), myeloid and plasmacytoid dendritic cells (mDCs and pDCs, respectively) interacted with GO-In (**Figure 1f, 1g** and **1h**).

To improve the resolution of our analysis, we performed a computational viSNE analysis on gated monocytes subpopulations (CD3-, CD19-, CD11c+), applying CD14, CD16, HLA-DR, and CD11c as clustering markers. Gating strategy of monocyte subpopulations is shown in **Figure S4**. The single-cell view confirmed that C. monocytes interacted the most with GO-In, showing possible heterogeneity among the subpopulations with possible range of interactions strength among cells (**Figure 2a**). Int. monocytes and NC monocytes had a low interaction with GO-In (**Figure 2a**). The bar graph better shows this phenomenon among the three subpopulations (**Figure 2b**). Intriguingly, the differences in interaction among and within the cell subpopulations do not correlate with a loss of cell viability (**Figure 2c** and **2d**). Instead, the opposite is might be true for C. monocytes, cisplatin signal for viability was inversely correlated with positive signal for GO-In (**Figure 2d and Figure S5)**. We next analyzed the GO-In impact on functionality of C. monocytes. No significant differences on activation marker expression was detected (**Figure 2e**). Moreover, we found a reduction of MIP1β and TNFα signal in GO-In treated cells, suggesting that GO-In does not induce C. monocyte activation (**Figure 2f**).

Next, we investigated whether B cell subpopulations responded differently to GO-In. We performed an extensive viSNE analysis on gated B cells applying CD19, CD20, CD27 and HLA-DR as markers. We successfully characterized at single-cell level the Naïve, memory, and plasma B cells (**Figure S6**). GO-In interacted significantly with all three subpopulations (**Figure 3a** and **3b**). But no significant differences on GO-In interaction were present between the three subpopulations, suggesting that no particular B cell differentiation state is needed for

their interaction with GO-In (**Figure 3b**). The intrinsic antigen presentation activity played by B cells *in vivo* [49] might explain the absence of strong interaction differences among the three subpopulations. However, the GO-In contact seems to be diverse on a single-cell base, showing a strong heterogeneity among the cells (**Figure 3a**). To this extent, no loss on viability is reported among untreated and treated cells (**Figure 3c** and **3d**). However, among the naïve B cells, we found an increased toxicity in the cells positive for GO-In compared to the negative cells (**Figure S7**). A similar trend, but not statistically significant, was also present on memory and plasma B Cells (**Figure S7**). Single-cell mass cytometry allowed us to study both the interaction with GO-In and how this affects the response of B cells. We found that GO-In stimulated the expression of CD25 in all three B subpopulations (**Figure 3e**). CD86 instead was only increased in the memory subpopulation (**Figure 3e**). Furthermore, the cytokine expression analysis (**Figure 3f**) suggested that naïve and memory B cells are the population strongly affected by the GO-In interaction with a significant expression of MIP1β, also known as CCL4 (**Figure 3f)** and a not significant increase of IL2. CCL4 secreted by activated B cells and other antigen presenting cells (APC) like macrophages and DCs is known to be a potent attractant for CD4+ T cells. The interaction between B and T cells is a critical determinant of the activation and/or control of the immunological response [50].

To prove that the effects that we observed on monocytes and B cell were not due to the QDs, the viability, activation and cytokine release were measured on the isolated cell populations (**Figure S8 and S9**). We have found that In quantum dots alone have negligible effects on monocyte and B cell viability, activation and cytokine expression.

In this work, the study at high dimensional single-cell level of the immune cell functional responses to graphene oxide was unrestricted by the inherent limitation due to the nanomaterial mass in CyTOF. As a proof of concept, our approach to graphene tracking, via indium conjugation, provides a versatile strategy to investigate nanomaterial safety. Several are the reasons why we expect that a deeper meaning of this pilot study will reveal many unexpected

views in graphene and other nanomaterials safety. Here we offer an opportunity to perform large in-depth graphene material screening to investigate the mechanism underlying the impact of graphene forms on immune cells by following graphene interactions. Indeed, graphene, in its multiple forms, has several physicochemical parameters that should be taken into consideration exploiting its potential impact on human health, including the lateral dimension, carbon/oxygen ratio and number of layers [51]. Single-cell mass cytometry has been successfully applied in neuroscience [31, 32, 52, 53], considering the applications of graphene as neuronal device [47, 54] an extension of our approach can be applicable to this specific research area. Finally, our GO-In can be easily translated into biodistribution studies at the tissue levels, using the recent developments in imaging single-cell mass cytometry [55, 56]. Moreover, the expansion of our "tracking approach" to other emerging 2D materials [57-59] will enable to faster their toxicological insights likely advancing new discoveries in nanotechnology.

In conclusion, going far beyond traditional toxicological methods, we propose a new system-wide approach based on single-cell mass cytometry as a reliable and sensitive tool to track graphene material interactions in biology and biomedicine. Single-cell mass cytometry has become in ten years an established platform of groundbreaking discoveries in biology. By taking full advantage of this high-dimensional single-cell technique, we will likely reach the same for graphene and 2D materials in nanotechnology.

Experimental section

Methods

Transmission electron microscopy analyses were performed with a Hitachi H7500 transmission electron microscope (Hitachi High Technologies Corporation, Tokyo, Japan) with an accelerating voltage of 80 kV equipped with an AMT Hamamatsu digital camera (Hamamatsu

Photonics, Hamamatsu City, Japan). The samples were dispersed in water and drop-casted onto a carbon-coated copper grid (Formvar/Carbon 300 Mesh, Cu from Delta Microscopies) and left for evaporation under ambient conditions. X-ray photoelectron spectroscopy (XPS) was performed on a Thermo Scientific K-Alpha X-ray photoelectron spectrometer with a basic chamber pressure of 10^{-8}-10^{-9} bar and an Al anode as the X-ray source (1486 eV). The samples were analyzed as powder or deposited on a support *via* drop-casting on a silicon wafer coated with SiO_2 (200 nm ± 5% of SiO_2, Tedpella 21620-6) Spot size of 400 μm was used. The survey spectra are average of 10 scans with a pass energy of 200.00 eV and a step size of 1 eV.

Material preparation

GO were purchased from NanoInnova Inc. (Spain). Aqueous suspensions were prepared by dispersing the powder in water and sonicating for 20 min prior to use. $AgInS_2$ QDs were synthesized by controlled decomposition method as we already reported [47, 48]. For the synthesis of the QDs, 17 mg of $AgNO_3$ (0.1 mmol, Sigma-Aldrich) and 88.4 mg of $InCl_3$ (0.4 mmol, Sigma-Aldrich) were placed in a 100 mL round-bottom flask. Then, 190 μL of oleic acid (0.6 mmol, Sigma-Aldrich), 720 μL of dodecylthiol (0.6 mmol, Sigma-Aldrich), and 8 mL of 1-octadecene (Sigma-Aldrich) were added under argon. The solution was heated at 60°C for 15 min, at 90°C for 15 min, and left at 110°C stirring until no precipitate was visible (15−30 min). Then, 4 mL of solution of elemental sulfur (9.6 mg 0.3 mmol, Sigma-Aldrich) was added and the mixture turned reddish. After 15 min, the reaction was cooled with an ice bath. The QDs were purified by precipitation with ethanol, resuspended with cyclohexane, washed several times with ethanol/acetone and stored in CH_2Cl_2. For the water transfer reaction, 2 mL of solution oil QDs (2 mg/mL dispersion) was added to 1 mL of a cysteine (50 mg, 0.4 mmol) basic (75 mg of KOH per ml) solution in methanol. Immediately, the QD precipitated. After 20 min, 5 mL of distilled water was added and the QD passed in the aqueous phase. Subsequently, the water-soluble QDs were precipitated with acetone, washed several times with

acetone/ethanol, and stored in distilled water. For GO conjugation, the QDs were mixed with GO (1 mg/mL) at 1:10 mass ratio in distilled water. The mixture was left stirring for 3 days and then purified by dialysis against distilled water.

Stability assays

GO-In stability in cell culture media was assayed incubating the nanomaterial at a concentration of 100 µg/mL at 37°C for one week and observed by TEM.

Cell Culture

Buffy coats from informed healthy donors (aged 25–50 years) were obtained from the University Hospital Tor Vergata and University Hospital of Sassari. Informed signed consent was obtained from all the donors. Human peripheral blood mononuclear cells (PBMCs) were isolated from buffy coat by Ficoll-Paque PLUS (GE Healthcare) density gradient centrifugation. PBMCs were maintained in RPMI-1640 medium added with FBS 10% and 1% of penicillin/streptomycin solution. At least 1×10^6 cells for sample in each experiment were used. All the experiments were performed in biological and technical triplicate.

GO-In tracking on human PBMCs by CyTOF2

Single-cell mass cytometry analysis was performed using purified PBMCs obtained as described above. PBMCs were seeded in a six multi-well plates (3×10^6 cells/well) and treated with GO-In at the fixed concentration of 50 µg/ml for 24 h or left untreated. For the detection of cytokines, brefeldin A was added 5hrs before the incubation end. Cell staining, acquisition and analysis were performed as previously described [17].

Gating strategy and statistical analysis methods applied

The analysis of CyTOF data was performed as previously described by Bendall *et al. [23]* and us [17]. Normalized, background subtracted FCS files were imported into Cytobank for analysis. Cell events were gated excluding the cell debris, doublets, and dead cells using the Cell-ID Intercalator-Ir and Cis. We defined specific PBMC subsets and subpopulations as reported previously [17]. New gating strategy used in the present paper are reported in Supplementary Figure 1 and 3.

Flow cytometer analyses

Monocytes and B cells were isolated from healthy donor PBMCs using the respective kits (#130-050-201 and #130-091-151, Miltenyi Biotec) according to the manufacturer's instructions. Viability and activation of monocytes and B cells were assessed using flow cytometry (Beckman Coulter Gallios). Cells were washed with 2% FBS in PBS (FACS Buffer), then stained with the respective antibody mix at 4 °C for 20 min. The anti-human antibodies used were CD25-APC (Miltenyi Biotec, #130-109-021), CD80-PE (BD, #557227) and CD86-FITC (BD, #555657). Viability of cells was analysed by staining with Fixable Viability Dye (eBioscience FVD-eFluor 780, #65-0865-14). After staining, cells were washed twice with FACS buffer, then resuspended in FACS buffer and analysed on the flow cytometer.

ELISA

Secretion of the cytokines IL-1β (BD Opt-EIA #557953), TNF (BD Opt-EIA #555212) were assayed with ELISA kits according to the manufacturer's instructions. In short, polyvinyl microtiter 96-well plates (Falcon) were coated overnight at 4 °C with 50 µl/well of purified capture antibodies diluted in coating buffer (carbonate/bicarbonate buffer 0.05M, pH 9.6). After washing with PBS containing 0.05% Tween (PBS-T), a blocking step was performed by adding 5% FBS in PBS (100 µl/well) for 1 h at room temperature. After washing thrice with PBS-T, 50 µl of culture supernatants were added in the respective wells for 2 h at room temperature,

along with a respective series of standards as provided in the kits. The plates were then washed five times with PBS-T. Secondary antibodies as provided in the kit were then added together with HRP reagent and incubated for 1 h at room temperature. Then, the plates were washed five times with PBS-T, and the presence of cytokines in the tested supernatants was visualized by adding tetramethylbenzidine (TMB) in the presence of H_2O_2. The resulting absorbance was measured at 450 nm after stopping the reaction with 2 N H_2SO4, after 15 min.

Supporting Information

Supporting Information is available from the Wiley Online Library or from the author.

Acknowledgments

This work was partly supported by the European Union's Horizon 2020 research and innovation programme under the Marie Sklodowska-Curie grant agreement no. 734381 (CARBO-IMmap), and FLAGERA JTC Graphene 2015 (G-IMMUNOMICS project), and the Agence Nationale de la Recherche (ANR) through the LabEx project Chemistry of Complex Systems (ANR-10-LABX-0026_CSC). The authors gratefully acknowledge the financial support from the EU GRAPHENE Flagship project (no. 785219). The authors wish to thank C. Royer and V. Demais for TEM analyses at the Plateforme Imagerie in Vitro at the INCI (Strasbourg, France).

References

1. Geim, A. K.; Novoselov, K. S., *Nat Mater* **2007,** *6* (3), 183-91.

2. Geim, A. K., *Science* **2009,** *324* (5934), 1530-4.

3. Brumfiel, G., *Nature* **2009,** *458* (7237), 390-1.

4. Novoselov, K. S.; Fal'ko, V. I.; Colombo, L.; Gellert, P. R.; Schwab, M. G.; Kim, K., *Nature* **2012,** *490* (7419), 192-200.

5. Kong, W.; Kum, H.; Bae, S. H.; Shim, J.; Kim, H.; Kong, L.; Meng, Y.; Wang, K.; Kim, C.; Kim, J., *Nat Nanotechnol* **2019,** *14* (10), 927-938.

6. Gazzi, A.; Fusco, L.; Khan, A.; Bedognetti, D.; Zavan, B.; Vitale, F.; Yilmazer, A.; Delogu, L. G., *Front Bioeng Biotechnol* **2019,** *7*, 295.

7. Orecchioni, M.; Cabizza, R.; Bianco, A.; Delogu, L. G., *Theranostics* **2015,** *5* (7), 710-23.

8. Reina, G.; Gonzalez-Dominguez, J. M.; Criado, A.; Vazquez, E.; Bianco, A.; Prato, M., *Chem Soc Rev* **2017,** *46* (15), 4400-4416.

9. Cheng, L.; Wang, X.; Gong, F.; Liu, T.; Liu, Z., *Adv Mater* **2019**, e1902333.

10. Fadeel, B.; Bussy, C.; Merino, S.; Vazquez, E.; Flahaut, E.; Mouchet, F.; Evariste, L.; Gauthier, L.; Koivisto, A. J.; Vogel, U.; Martin, C.; Delogu, L. G.; Buerki-Thurnherr, T.; Wick, P.; Beloin-Saint-Pierre, D.; Hischier, R.; Pelin, M.; Candotto Carniel, F.; Tretiach, M.; Cesca, F.; Benfenati, F.; Scaini, D.; Ballerini, L.; Kostarelos, K.; Prato, M.; Bianco, A., *ACS Nano* **2018,** *12* (11), 10582-10620.

11. Feliu, N.; Fadeel, B., *Nanoscale* **2010,** *2* (12), 2514-20.

12. Damoiseaux, R.; George, S.; Li, M.; Pokhrel, S.; Ji, Z.; France, B.; Xia, T.; Suarez, E.; Rallo, R.; Madler, L.; Cohen, Y.; Hoek, E. M.; Nel, A., *Nanoscale* **2011,** *3* (4), 1345-60.

13. Galli, E.; Friebel, E.; Ingelfinger, F.; Unger, S.; Nunez, N. G.; Becher, B., *Eur J Immunol* **2019,** *49* (2), 212-220.

14. Spitzer, M. H.; Nolan, G. P., *Cell* **2016,** *165* (4), 780-91.

15. Bengt, F., *Frontiers in Toxicology* **2019,** *1*, 1.

16. Kunz, D. J.; Gomes, T.; James, K. R., *Front Immunol* **2018,** *9*, 1435.

17. Orecchioni, M.; Bedognetti, D.; Newman, L.; Fuoco, C.; Spada, F.; Hendrickx, W.; Marincola, F. M.; Sgarrella, F.; Rodrigues, A. F.; Menard-Moyon, C.; Cesareni, G.; Kostarelos, K.; Bianco, A.; Delogu, L. G., *Nat Commun* **2017,** *8* (1), 1109.

18. Finotello, F.; Rieder, D.; Hackl, H.; Trajanoski, Z., *Nat Rev Genet* **2019,** *20* (12), 724-746.

19. Palit, S.; Heuser, C.; de Almeida, G. P.; Theis, F. J.; Zielinski, C. E., *Front Immunol* **2019,** *10*, 1515.

20. Lakshmikanth, T.; Olin, A.; Chen, Y.; Mikes, J.; Fredlund, E.; Remberger, M.; Omazic, B.; Brodin, P., *Cell Rep* **2017,** *20* (9), 2238-2250.

21. Bandura, D. R.; Baranov, V. I.; Ornatsky, O. I.; Antonov, A.; Kinach, R.; Lou, X.; Pavlov, S.; Vorobiev, S.; Dick, J. E.; Tanner, S. D., *Anal Chem* **2009,** *81* (16), 6813-22.

22. Bjornson, Z. B.; Nolan, G. P.; Fantl, W. J., *Curr Opin Immunol* **2013,** *25* (4), 484-94.

23. Bendall, S. C.; Simonds, E. F.; Qiu, P.; Amir el, A. D.; Krutzik, P. O.; Finck, R.; Bruggner, R. V.; Melamed, R.; Trejo, A.; Ornatsky, O. I.; Balderas, R. S.; Plevritis, S. K.; Sachs, K.; Pe'er, D.; Tanner, S. D.; Nolan, G. P., *Science* **2011,** *332* (6030), 687-96.

24. Brodin, P.; Jojic, V.; Gao, T.; Bhattacharya, S.; Angel, C. J.; Furman, D.; Shen-Orr, S.; Dekker, C. L.; Swan, G. E.; Butte, A. J.; Maecker, H. T.; Davis, M. M., *Cell* **2015,** *160* (1-2), 37-47.

25. Kaczorowski, K. J.; Shekhar, K.; Nkulikiyimfura, D.; Dekker, C. L.; Maecker, H.; Davis, M. M.; Chakraborty, A. K.; Brodin, P., *Proc Natl Acad Sci U S A* **2017,** *114* (30), E6097-E6106.

26. Olin, A.; Henckel, E.; Chen, Y.; Lakshmikanth, T.; Pou, C.; Mikes, J.; Gustafsson, A.; Bernhardsson, A. K.; Zhang, C.; Bohlin, K.; Brodin, P., *Cell* **2018,** *174* (5), 1277-1292 e14.

27. Wong, M. T.; Ong, D. E.; Lim, F. S.; Teng, K. W.; McGovern, N.; Narayanan, S.; Ho, W. Q.; Cerny, D.; Tan, H. K.; Anicete, R.; Tan, B. K.; Lim, T. K.; Chan, C. Y.; Cheow, P. C.; Lee, S. Y.; Takano, A.; Tan, E. H.; Tam, J. K.; Tan, E. Y.; Chan, J. K.; Fink, K.; Bertoletti, A.; Ginhoux, F.; Curotto de Lafaille, M. A.; Newell, E. W., *Immunity* **2016,** *45* (2), 442-56.

28. Chevrier, S.; Levine, J. H.; Zanotelli, V. R. T.; Silina, K.; Schulz, D.; Bacac, M.; Ries, C. H.; Ailles, L.; Jewett, M. A. S.; Moch, H.; van den Broek, M.; Beisel, C.; Stadler, M. B.; Gedye, C.; Reis, B.; Pe'er, D.; Bodenmiller, B., *Cell* **2017,** *169* (4), 736-749 e18.

29. Lavin, Y.; Kobayashi, S.; Leader, A.; Amir, E. D.; Elefant, N.; Bigenwald, C.; Remark, R.; Sweeney, R.; Becker, C. D.; Levine, J. H.; Meinhof, K.; Chow, A.; Kim-Shulze, S.; Wolf, A.; Medaglia, C.; Li, H.; Rytlewski, J. A.; Emerson, R. O.; Solovyov, A.; Greenbaum, B. D.; Sanders, C.; Vignali, M.; Beasley, M. B.; Flores, R.; Gnjatic, S.; Pe'er, D.; Rahman, A.; Amit, I.; Merad, M., *Cell* **2017,** *169* (4), 750-765 e17.

30. Newell, E. W.; Sigal, N.; Nair, N.; Kidd, B. A.; Greenberg, H. B.; Davis, M. M., *Nat Biotechnol* **2013,** *31* (7), 623-9.

31. Ajami, B.; Samusik, N.; Wieghofer, P.; Ho, P. P.; Crotti, A.; Bjornson, Z.; Prinz, M.; Fantl, W. J.; Nolan, G. P.; Steinman, L., *Nat Neurosci* **2018,** *21* (4), 541-551.

32. Mrdjen, D.; Pavlovic, A.; Hartmann, F. J.; Schreiner, B.; Utz, S. G.; Leung, B. P.; Lelios, I.; Heppner, F. L.; Kipnis, J.; Merkler, D.; Greter, M.; Becher, B., *Immunity* **2018,** *48* (2), 380-395 e6.

33. Landhuis, E., *Nature* **2018,** *557* (7706), 595-597.

34. Yang, Y. S.; Atukorale, P. U.; Moynihan, K. D.; Bekdemir, A.; Rakhra, K.; Tang, L.; Stellacci, F.; Irvine, D. J., *Nat Commun* **2017,** *8*, 14069.

35. Ivask, A.; Mitchell, A. J.; Hope, C. M.; Barry, S. C.; Lombi, E.; Voelcker, N. H., *Anal Chem* **2017,** *89* (16), 8228-8232.

36. Lopez-Serrano Oliver, A.; Haase, A.; Peddinghaus, A.; Wittke, D.; Jakubowski, N.; Luch, A.; Grutzkau, A.; Baumgart, S., *Anal Chem* **2019,** *91* (18), 11514-11519.

37. Ha, M. K.; Kwon, S. J.; Choi, J. S.; Nguyen, N. T.; Song, J.; Lee, Y.; Kim, Y. E.; Shin, I.; Nam, J. W.; Yoon, T. H., *Small* **2020**, e1907674.

38. Bitounis, D.; Ali-Boucetta, H.; Hong, B. H.; Min, D. H.; Kostarelos, K., *Adv Mater* **2013,** *25* (16), 2258-68.

39. Mukherjee, S. P.; Bottini, M.; Fadeel, B., *Front Immunol* **2017,** *8*, 673.

40. Rive, C.; Reina, G.; Wagle, P.; Treossi, E.; Palermo, V.; Bianco, A.; Delogu, L. G.; Rieckher, M.; Schumacher, B., *Small* **2019,** *15* (45), e1902699.

41. Liu, B.; Xie, J.; Ma, H.; Zhang, X.; Pan, Y.; Lv, J.; Ge, H.; Ren, N.; Su, H.; Xie, X.; Huang, L.; Huang, W., *Small* **2017,** *13* (18).

42. Wang, H.; Ma, K.; Xu, B.; Tian, W., *Small* **2016,** *12* (47), 6613-6622.

43. Xu, G.; Zeng, S.; Zhang, B.; Swihart, M. T.; Yong, K. T.; Prasad, P. N., *Chem Rev* **2016,** *116* (19), 12234-12327.

44. Mir, I. A.; Radhakrishanan, V. S.; Rawat, K.; Prasad, T.; Bohidar, H. B., *Sci Rep* **2018,** *8* (1), 9322.

45. Reina, G.; Chau, N. D. Q.; Nishina, Y.; Bianco, A., *Nanoscale* **2018,** *10* (13), 5965-5974.

46. Bordoni, V.; Reina, G.; Orecchioni, M.; Furesi, G.; Thiele, S.; Gardin, C.; Zavan, B.; Cuniberti, G.; Bianco, A.; Rauner, M.; Delogu, L. G., *Nanoscale* **2019,** *11* (41), 19408-19421.

47. Rauti, R.; Medelin, M.; Newman, L.; Vranic, S.; Reina, G.; Bianco, A.; Prato, M.; Kostarelos, K.; Ballerini, L., *Nano Lett* **2019,** *19* (5), 2858-2870.

48. Reina, G.; Ruiz, A.; Murera, D.; Nishina, Y.; Bianco, A., *ACS Appl Mater Interfaces* **2019,** *11* (8), 7695-7702.

49. Hong, S.; Zhang, Z.; Liu, H.; Tian, M.; Zhu, X.; Zhang, Z.; Wang, W.; Zhou, X.; Zhang, F.; Ge, Q.; Zhu, B.; Tang, H.; Hua, Z.; Hou, B., *Immunity* **2018,** *49* (4), 695-708 e4.

50. Bystry, R. S.; Aluvihare, V.; Welch, K. A.; Kallikourdis, M.; Betz, A. G., *Nat Immunol* **2001,** *2* (12), 1126-32.

51. Wick, P.; Louw-Gaume, A. E.; Kucki, M.; Krug, H. F.; Kostarelos, K.; Fadeel, B.; Dawson, K. A.; Salvati, A.; Vazquez, E.; Ballerini, L.; Tretiach, M.; Benfenati, F.; Flahaut, E.; Gauthier, L.; Prato, M.; Bianco, A., *Angew Chem Int Ed Engl* **2014,** *53* (30), 7714-8.

52. Lanz, T. V.; Probstel, A. K.; Mildenberger, I.; Platten, M.; Schirmer, L., *Front Immunol* **2019,** *10*, 1302.

53. Korin, B.; Ben-Shaanan, T. L.; Schiller, M.; Dubovik, T.; Azulay-Debby, H.; Boshnak, N. T.; Koren, T.; Rolls, A., *Nat Neurosci* **2017,** *20* (9), 1300-1309.

54. Sakai, K.; Teshima, T. F.; Nakashima, H.; Ueno, Y., *Nanoscale* **2019,** *11* (28), 13249-13259.

55. Damond, N.; Engler, S.; Zanotelli, V. R. T.; Schapiro, D.; Wasserfall, C. H.; Kusmartseva, I.; Nick, H. S.; Thorel, F.; Herrera, P. L.; Atkinson, M. A.; Bodenmiller, B., *Cell Metab* **2019,** *29* (3), 755-768 e5.

.

56. Giesen, C.; Wang, H. A.; Schapiro, D.; Zivanovic, N.; Jacobs, A.; Hattendorf, B.; Schuffler, P. J.; Grolimund, D.; Buhmann, J. M.; Brandt, S.; Varga, Z.; Wild, P. J.; Gunther, D.; Bodenmiller, B., *Nat Methods* **2014,** *11* (4), 417-22.

57. Jayakumar, A.; Surendranath, A.; Pv, M., *Int J Pharm* **2018,** *551* (1-2), 309-321.

58. Kostarelos, K., *Nat Rev Mater* **2016,** *1* (16084).

59. Taheri, H.; Unal, M. A.; Sevim, M.; Gurcan, C.; Ekim, O.; Ceylan, A.; Syrgiannis, Z.; Christoforidis, K. C.; Bosi, S.; Ozgenc, O.; Gomez, M. J.; Turktas Erken, M.; Soydal, C.; Eroglu, Z.; Bitirim, C. V.; Cagin, U.; Ari, F.; Ozen, A.; Kucuk, O.; Delogu, L. G.; Prato, M.; Metin, O.; Yilmazer, A., *Small* **2020,** *16* (10), e1904619.

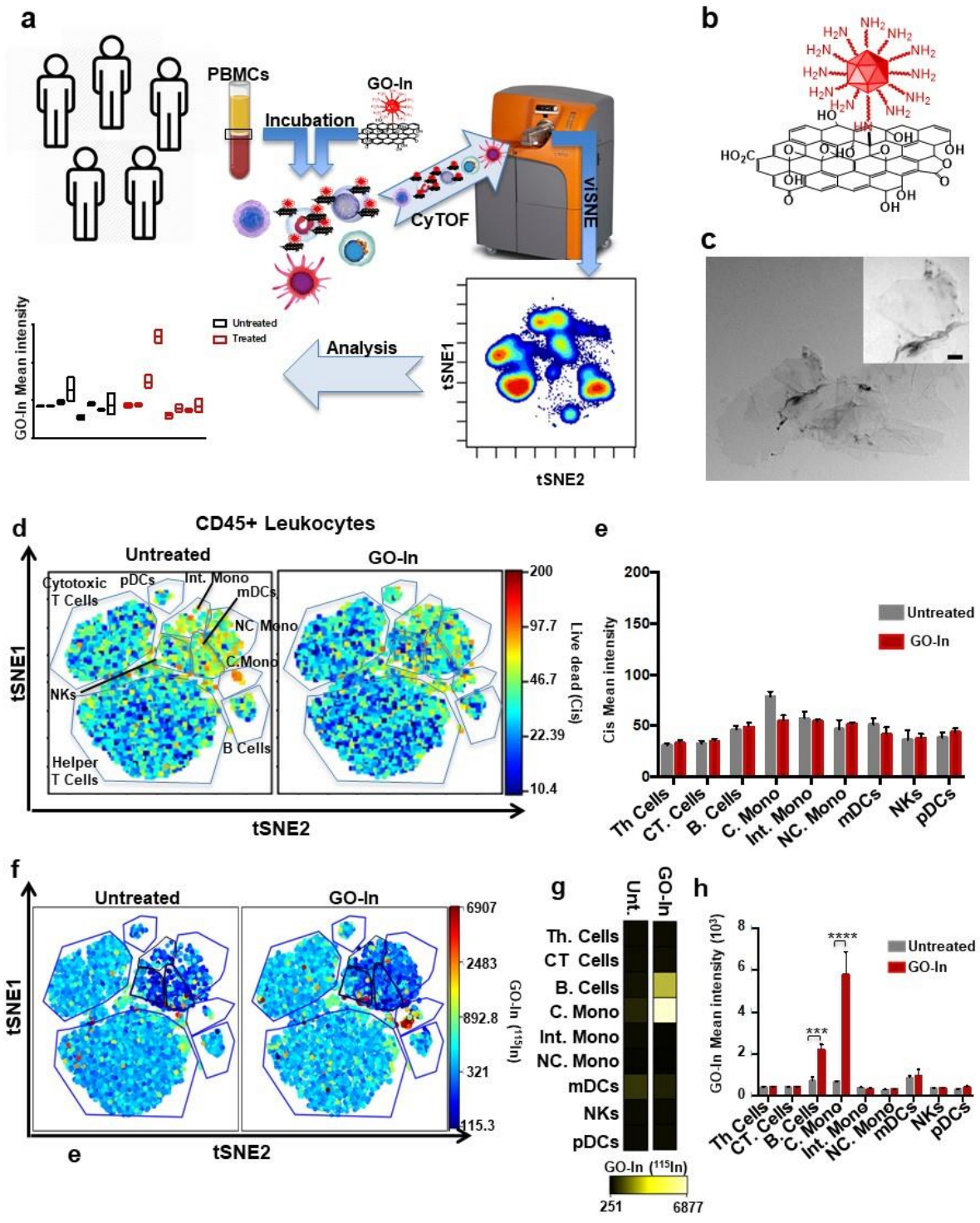

Figure 1. Single cell tracking analysis of GO-In on human PBMCs. a) Experimental plan and GO-In characterization. Blood from healthy donors was drawn and PBMCs were isolated incubated with GO-In and stained for mass cytometry analysis. **b**) Molecular structure of GO-In. **c**) TEM image of GO-In, scale bar 500 µm. Inset: higher magnification of the QDs onto the GO surface, scale bar 100 nm**. d**) Cell viability analysis using Cisplatin (Cis) reagent with CyTOF. Plots show the use of viSNE to obtain a comprehensive single-cell view and to distinguish the PBMC subpopulations. **e**) The bar graph reports the Cis median intensity in all

subpopulations identified. **f**) viSNE plots showing the GO-In mean intensity in treated (50µg/mL) and untreated immune subpopulations. **g**) Representative heat map and **h**) Bar graph reporting the GO-In mean intensity in all subpopulations identified. GO-In internalization intensity is represented form blue (low internalization) to red (high internalization). All the experiments were performed in triplicate and shown as means±SD. **P*<0.05; ***P*<0.01, ****P*<0.001 by one-way ANOVA and student T Test when appropriate.

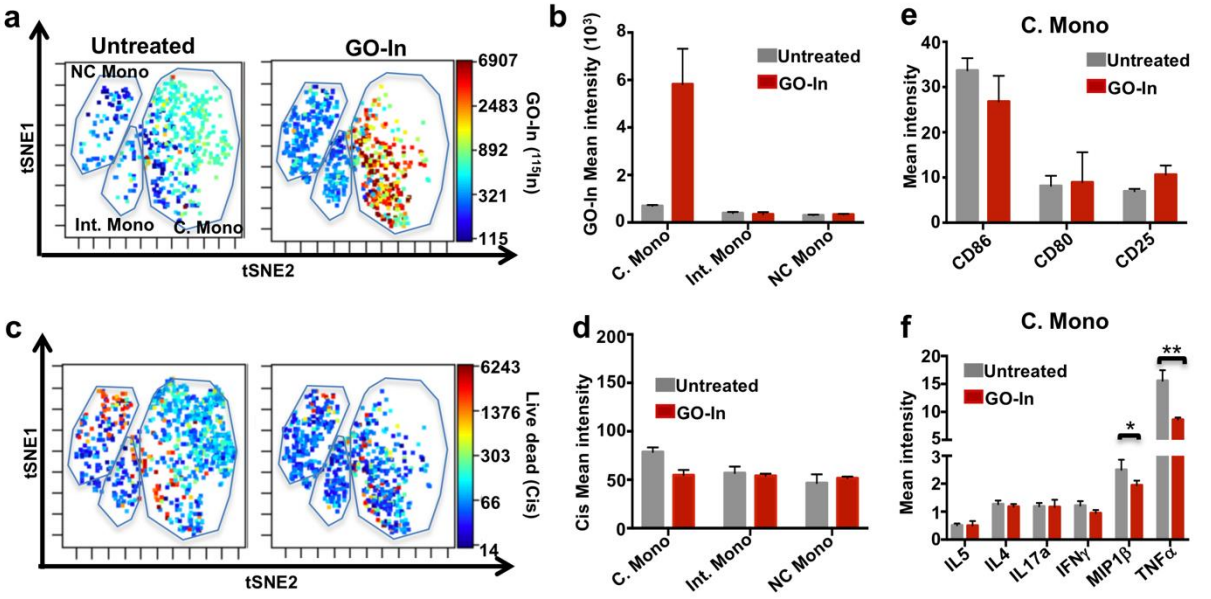

Figure 2. GO-In tracking on human monocyte subpopulations. **a**) viSNE visualization of monocytes subpopulations, Classical (C), Intermediate (Int) and Non-Classical (NC) are reported. **b**) Bar graph showing the GO-In mean intensity in all Monocytes subpopulations for treated or untreated cells. **c**) viSNE visualization of monocytes viability analysis using Cis reagent. **d**) Bar graph reporting the Cis mean intensity. **e**) Bar graphs showing the mean expression ratio of CD86, CD80 and CD25 activation marker for gated C. Monocytes treated or untreated with GO-in. **f**) Analysis of IL5, IL4, IL17a, IFNg, MIP1b and TNF cytokines expression on C. monocytes. All the experiments were performed in triplicate and shown as means± SD. **P*<0.05; ***P*<0.01, ****P*<0.001 by one-way ANOVA and student T Test when appropriate.

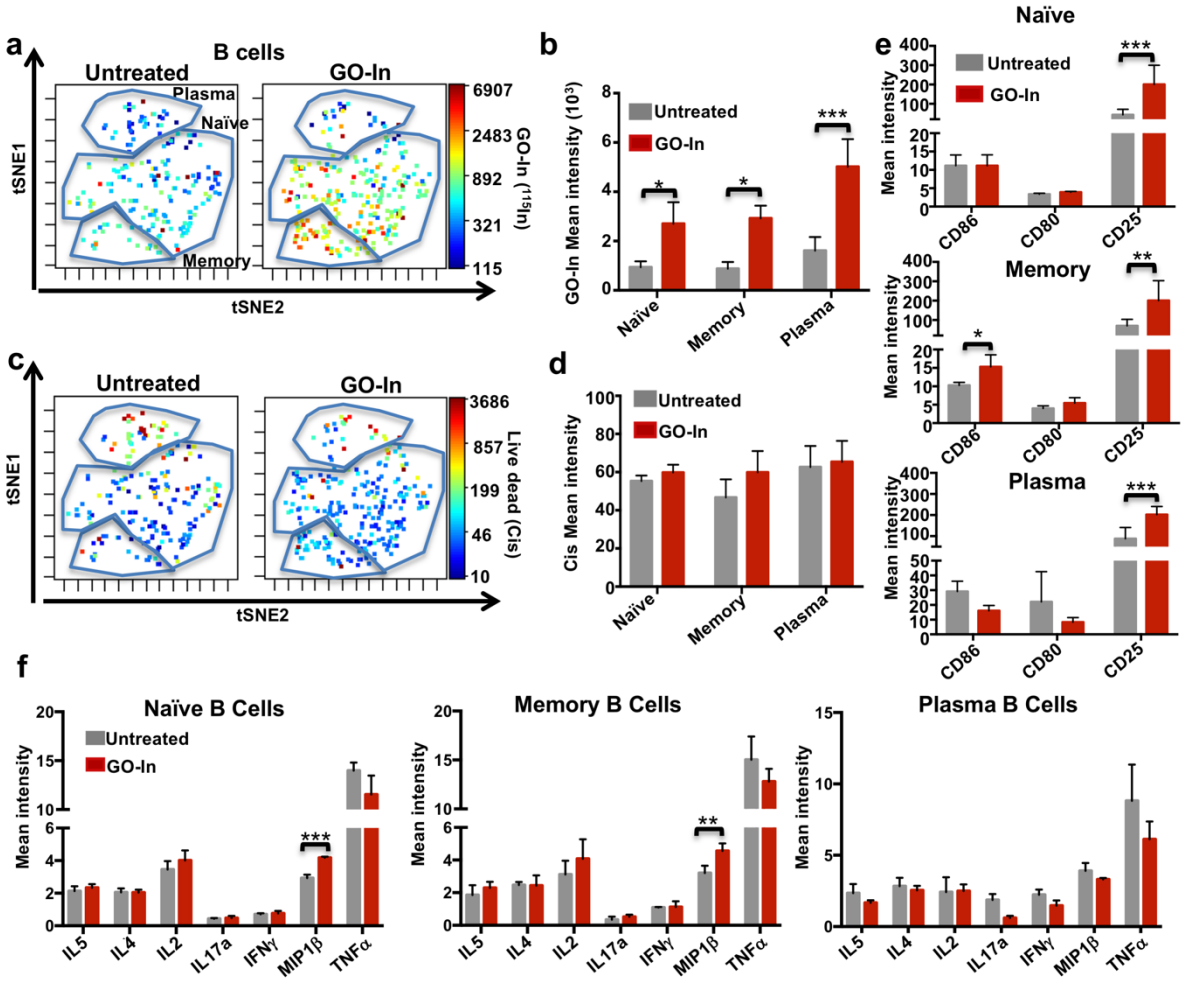

Figure 3. GO-In tracking on human B cell subpopulations. a) viSNE visualization of B Cells subpopulations (Naïve, Memory and Plasma). **b**) Bar graph reporting the GO-In mean intensity in all B Cell subpopulations identified. **c)** Cell viability analysis using Cis reagent. **d**) Bar graph reports the Cis mean intensity. **e**) Activation marker analysis on B cells subpopulations treated or untreated with GO-In. **f**) IL5, IL4, IL2, IL17a, IFNg, MIP1b and TNFa mean expression is reported. All the experiments were performed in triplicate and shown as means± SD. **P*<0.05; ***P*<0.01, ****P*<0.001 by one-way ANOVA and student T Test when appropriate.

TOC

A versatile strategy to investigate nanomaterials safety

